ResearchGate

See discussions, stats, and author profiles for this publication at: https://www.researchgate.net/publication/264562199

First Principles Study of Morphology, Doping Level, and Water Solvation Effects on the Catalytic Mechanism of Nitrogen-Doped Graphene in the Oxygen Reduction Reaction

ARTICLE *in* CHEMCATCHEM · SEPTEMBER 2014

Impact Factor: 4.56 · DOI: 10.1002/cctc.201402248

CITATIONS
3

READS
74

5 AUTHORS, INCLUDING:

Seung Hyo Noh
Tokyo Institute of Technology
11 PUBLICATIONS **68** CITATIONS
SEE PROFILE

Byungchan Han
Yonsei University
37 PUBLICATIONS **506** CITATIONS
SEE PROFILE

Available from: Byungchan Han
Retrieved on: 26 January 2016

Manuscript
Click here to download Manuscript: ChemCatChem_Manuscript.docx

DOI: 10.1002/cctc.200((will be filled in by the editorial staff))

First Principles Study of Morphology, Doping Level and Water Solvation Effects on Catalytic Mechanism of a Graphene Towards Oxygen Reduction Reaction

Dohyun Kwak[a], Abhishek Khetan[b], Seunghyo Noh[c], Heinz Pitsch[b], Byungchan Han*[a]

First principles density functional theory calculations are utilized to unveil oxygen reduction reaction mechanisms on nitrogen doped graphene (N-Gr). Considering the effect of both the geometry and concentration of N in bulk and edge N-Gr forms, we calculate the energies of a large number of model systems to cover a wide range of possible N-Gr structures and determine the most stable ones. In agreement with experiments, our calculations suggest that doping levels in stable N-Gr forms are limited to less than about 30 at.%, above which the hexagonal graphene framework is broken. Remarkably, the ground state structures of bulk and edge N-Gr are found to differ depending on the doping level and poisoning of the edge bonds. ORR mechanisms are estimated using Gibbs free energy diagrams, both with and without water solvation. Our results indicate that N doping significantly alters the catalytic properties of pure graphene and that dilutely doped bulk N-Gr forms are the most active.

Introduction

Securing renewable energy sources is one of the most urgent challenges of our century. Fossil fuels are a limited resource and their use often has serious environmental impacts. As a result there has been a major drive recently to advance science and technology for harvesting green and renewable energies using, for instance the chemical energies of hydrogen and oxygen, photons, or biomass, Well to device energy conversion efficiencies of current processes in these fields, however, are still too low to be utilized for any practical-scale purpose and are often hampered by imperfect catalyst materials.

Efficiency of reducing oxygen plays a key role in controlling over all performances of energy systems in many industrial sectors, for instance, fuel generation devices,[1, 2] metal-air batteries,[3-5] and fuel cells[6-8] etc. One of the best examples is the Proton Exchange Membrane (PEM) fuel cell. In spite of its highly expected and theoretically possible high thermodynamic efficiency and environmentally friendly nature, ORR catalysts in the system still depend on pure or alloys of Pt, which is quite expensive and provides efficiencies that are not high enough to compete with conventional fossil fuel energy systems.

Doping pure substances with heteroatoms, by even very small amounts, often gives rise to material properties that are very different from those of the parent materials. This approach has been widely applied for devices such as semi-conductors, sensors and energy systems.[9-13]

Graphene doped with nitrogen atoms, or N-Gr, is considered a very promising material for replacing the costly Pt based metallic catalysts, since it has been discovered to show a markedly increased ORR activity as compared to pristine graphene.[14-16] In addition, N-Gr has been found to be much more stable against peroxides and takes part in the ORR reaction via a four-electron process, ultimately yielding water.[15-17] This implies that doping can completely modify the electronic structure or ORR mechanism of pristine graphene, which was confirmed in a study by Qu et al.,[16] who reported that pure graphene showed a two-step, two-electron process for oxygen reduction with low onset potential (-0.45 V and -0.7 V vs Ag/AgCl), while N-Gr exhibited a four-electron pathway with activity three times higher than Pt/C in alkaline media.

However, the oxygen reduction reaction (ORR) mechanisms in N-Gr are not clearly understood, as manifested in the widely scattered and inconclusive data consisting of both experimental measurements and theoretical calculations. For example, experimentally measured and calculated onset potentials for ORR

[a] *Mr. D. H. Kwak, Prof. B. C. Han*
Department of Energy Systems Engineering
Daegu Gyeongbuk Institute of Science and Technology (DGIST)
Daegu 711-873, Republic of Korea
Fax: (+82) 53-785-6412
E-mail: hanbc@dgist.ac.kr
[b] *Mr. A. Khetan, Prof. H.Pitsch*
Institute for Combustion Technology
RWTH Aachen University
Templergraben 64
D-52056 Aachen, Germany
[c] *Mr. S. H. Noh*
Department of Electronic Chemistry
Tokyo Institute of Technology
4259-G1-5 Nagatsuta,Midori-ku, Yokohama, 226-8502, Japan

in N-Gr have been reported in the range of 0.5 ~ 0.9 V (vs. NHE).[15-22] Moreover, there are a variety of suggestions for the ORR mechanisms underlying the catalytic activity. Kim et al.[23] proposed that the morphology of N-Gr (i.e., edge or bulk) is vital for controlling ORR activity, while Okamoto[24] has argued that the concentration of dopant N atoms around the C atom is the key to understanding ORR. Independent of the arguments based on structure, it has also been suggested that the activity could be attributed to delocalization of electronic charge in the C atoms neighbouring the dopant N atom.[25, 26] These properties of N-Gr make it especially attractive as an option for replacing costly Pt-based metallic catalysts in PEM Fuel cells.[17]

Development of highly functional doped N-Gr requires an accurate understanding of the underlying mechanisms using well-defined model systems and fundamental tools. To accomplish this goal, we utilize first principles density functional theory (DFT) calculations to bulk and edged forms of N-Gr, with varying N doping level. By rigorously screening approximately 900 N-Gr model systems, we will first identify the thermodynamically favoured ground state structures. Furthermore, we will evaluate the onset potentials for ORR on each of the structures by calculating the thermodynamic free energy diagrams and by taking into account the explicit effect of solvation due to water.

Results and Discussion

DFT calculations of stable N-Gr Structures

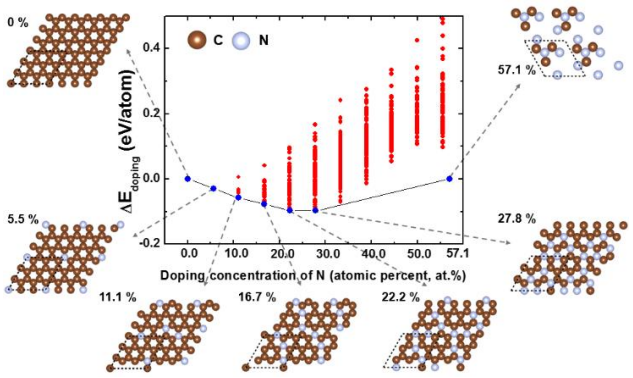

Figure 1. DFT calculated energy convex hull of 752 bulk N-doped graphene structures as a function of the doping level and arrangement of N and C atoms. Each N atom substitutes a C atom in (3x3) graphene sheets. The blue circles on the convex hull represent ground state structures at that given at.% N.

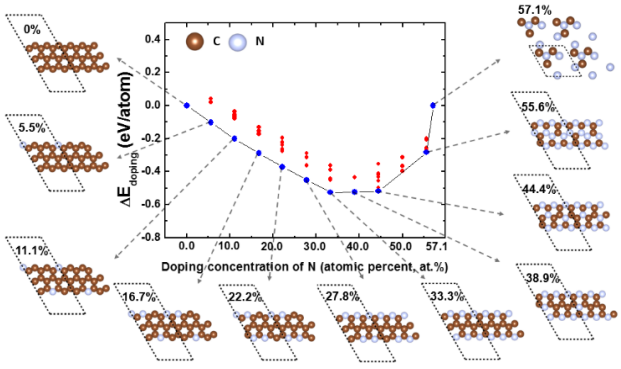

Figure 2. DFT calculated energy convex hull of 110 edge N-doped graphene model systems as a function of the doping level and relative arrangement of N and C atoms. The blue circles represent ground state structures that together form the energy convex hull as in Figure 1.

Using first principles DFT calculations for the ground state energy, we screened 752 bulk and 110 edge shapes of N-Gr as function of the dopant concentration and substitutional configuration. The numerous model systems were generated by employing computer programs based on the cluster expansion theory.[27] In such an approach, it is possible to have several structures having the same at.% N due to different relative arrangements of C and N atoms. The most stable structures at a given at.% N can be readily identified from the thermodynamic energy convex hull, which indicates the thermodynamically most plausible phase transition path among the calculated structures in the process of doping, as shown in Figure 1 for bulk and in Figure 2 for edge N-Gr.

The doping energy at an atomic percentage (at. %) of θ, $\Delta E_{doping}(\theta)$, of each N-Gr structure is defined as given in Eq. (1),

$$\Delta E_{doping}(\theta) = E(\theta) - \left\{ \left(E(\theta_{max}) - E(\theta_{min}) \right) \frac{\theta - \theta_{min}}{\theta_{max} - \theta_{min}} + E(\theta_{min}) \right\} \quad (1).$$

Here, θ is the at.% of a doped N with the corresponding values of θ_{min} and θ_{max} being 0 and 57.1 at. % N respectively. E(θ) is the DFT-calculated total energy for total energy for an N-Gr structure at θ. $E(\theta_{min})$ and $E(\theta_{max})$ are DFT-calculated energies for pristine graphene and carbon nitride (β-C_3N_4), and are used as reference models.[28] N-Gr with θ = 100 at.% N was not used as a reference because no such form has been reported in the literature until now. The doping energy ΔE_{doping} implies an amount of relative stabilization with respect to the hypothetical straight line connecting the energy levels of the two reference model systems. Understandably, the lower (more negative) is the doping energy at a given θ (or x), the higher is its relative stability.

Bulk N-Gr (graphitic N type) materials with θ below ~ 10 at.% N have been found in many experimental studies,[15-19] while higher θ are rarely reported. Souto et al.[29] have found that N-Gr materials with θ ≤ 20 at.% N maintain a graphite-like structure, and above this value they transform into the β-C_3N_4 phase due to the repulsive interaction between the lone-pairs in doped N. Our findings agree well with these observations as shown in Figure 1, where N-Gr structures with 5.5, 11.1, 16.7, 22.2, and 27.8 at.% N can be seen to be thermodynamically stable. In Figure 1, one can also clearly observe a two-phase equilibrium region from 27.8 to 57.1 at.% N, implying that structures in this region are thermodynamically unstable against decomposition into two N-Gr configurations with 27.8 and 57.1 at.% N. Relative amounts of the decomposed structures can be determined thermodynamically using the lever-rule. We found that the metastable hexagonal framework of the graphene sheet was destroyed due to strong repulsions between N atoms in this range of at.% N. Thus, the material no longer retains its original properties. These findings imply that thermodynamically, a doping level of ≤ 30 at.% N is feasible on graphene, above which the specific advantages of N-Gr as an ORR catalyst may disappear.

Figure 2 illustrates a similar DFT calculated energy convex hull for the edge forms of N-Gr, where we plot the doping energy as defined in Eq.1. Our results show that N-Gr structures with doping levels of 5.5, 11.1, 16.7, 22.2, 27.8, 33.3, 38.9, 44.4 and 55.6 at.% N are energetically stable. Above the 55.6 at.% N, however, the hexagonal framework of an edged N-Gr is broken due to strong repulsion between the lone pair electrons of the dopant N.

On comparing the magnitude of the doping energy, the edge N-Gr models can be predicted to be able to accommodate higher N

atoms than the bulk form. We propose that the reason for stability at relatively higher at.% N in edge N-Gr is at easier release of strain energy owing to the location of N atoms at undercoordinated sites, which is not facilitated in bulk form. Doped N atoms form a zigzag topology in edge N-Gr, which helps in overcoming the electrostatic repulsion between lone pairs from neighbouring N atoms. Predictably, one can assert that the experimental synthesis of edge N-Gr should be easier than the bulk form with increasing at.% N. This assertion is in excellent agreement with experimental results.[15, 21, 23]

Poisoning of dangling bonds in edge N-Gr

Before investigating ORR mechanisms in edge N-Gr model systems captured by the energy convex hull, as shown in Figure 2, we further thermodynamically studied whether atoms located at the edge boundaries (C and N), which have dangling bonds, are poisoned by the first ORR process. Specifically, we considered the electrochemical reaction of each the model systems with 5.5, 16.7 and 27.8 at.% N in edge N-Gr with ($H^+ + e^-$), and calculated the reversible potentials at T = 300 K, P = 1 atm and pH =0. The reversible potentials were calculated using Eq. (2) as:

$$U_{rev} = -\Delta G_{ads} / nF \qquad (2).$$

where U_{rev} and ΔG_{ads} are the reversible potential of the electrochemical reaction and change of Gibbs free energy during adsorption of H at the edge site, respectively. F is the Faraday constant and n is the number of electrons involved in the electrochemical reaction (here, n = 1). The change in zero point energy and entropy corrections were included in the Gibbs free energy change, as described in earlier studies.[30]

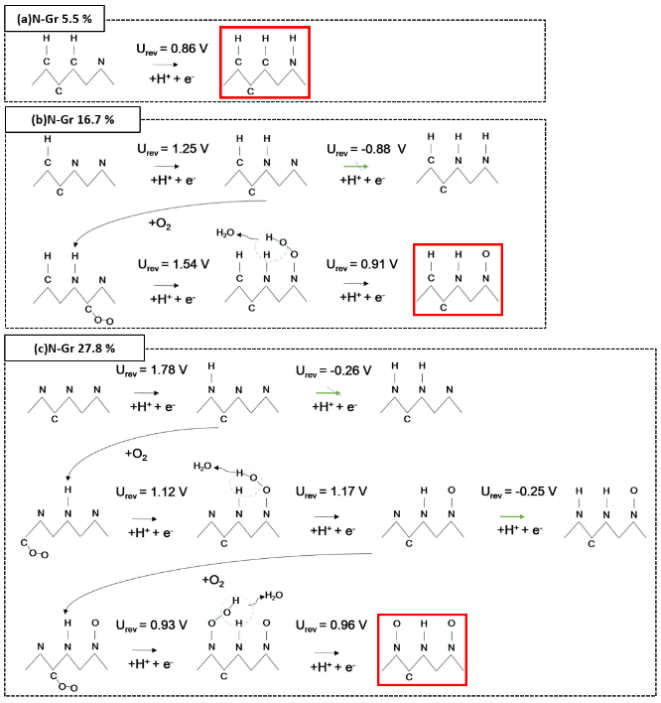

Figure 3. Schematic diagrams explaining the chain of reactions leading to the thermodynamically most stable configurations of edge N-Gr at (a) 5.5 at.% N, (b) 16.7 at.% N and (c) 27.8 at.% N. Each of the model systems was rigorously evaluated for adsorption by solvated protons and O_2 molecules. The reversible potentials for the electrochemical steps were identified using Eq. (2).

The first schematic, as shown in Figure 3(a), demonstrates how N and C atoms, located on the boundary in edge N-Gr with 5.5 at.% N, can form strong chemical bonds with H atoms at potentials below 0.86 V (vs SHE). Considering the fact that typical operational potentials of PEM fuel cells are below 0.8 ~ 0.9 V (vs SHE), H atoms poison all N atoms in edge N-Gr with 5.5 at.% N. Poisoning of these dangling bonds by either O or O_2 was not found to be thermodynamically more favourable than by H.

The process of H-poisoning becomes more complicated at higher at.% N. As can be seen in the schematic in Figure 3(b) at 16.7 at.% N, the edge C and its nearest neighbour N atoms can be expected to readily adsorb H atoms below the thermodynamic potential of PEM fuel cells (1.23 V at room temperature), while the other N atom prefers a state without adsorbed H. At the same time adsorption of O_2 at all possible positions was considered, but was found to be thermodynamically feasible only after removal of the dangling bond. In this structure, O_2 was found to preferentially adsorb on the graphitic C atom near N rather than N. Considering the high reduction potential (1.54 V), which is in fact within the potential window of oxygen gas evolution), however, the reduction of O_2 to OOH* is very strongly favoured to occur at the edge-located N atom, i.e., the N atom is thermodynamically the active site initiating O_2 reduction reaction. By searching for further thermodynamic reaction processes, we also find that the adsorbed OOH* can thermodynamically further dissociate into O* and OH* by reacting with yet another reduction on the N-Gr surface. Thus, the stable structure of N-Gr with 16.7 at.% N ends up with that marked by the red square at Figure 3(b).

Such phenomenon of the structural poisoning of dangling bonds by H or O atoms were also found by ab-initio calculations[31] and experimental measurements,[32, 33] which is consistent with the present observations.

Figure 3(c) shows the processes that leads to the thermodynamically stable configuration of the edge form of N-Gr at 27.8 at.% N, where all edge sites are occupied with N atoms. The thermodynamic path is similar to that of the 16.7 at.% N model: adsorbed O_2 molecules are reduced into OOH* at the N atom ending up poisoning two of three N atoms. One of the edge N forms chemical bonding with the adsorbed H atom. The reversible potentials are so high and within the windows of water stability regimes that the end-product structure may be quite stable at the PEM fuel cell operational condition as often observed in experiments.[32, 33]

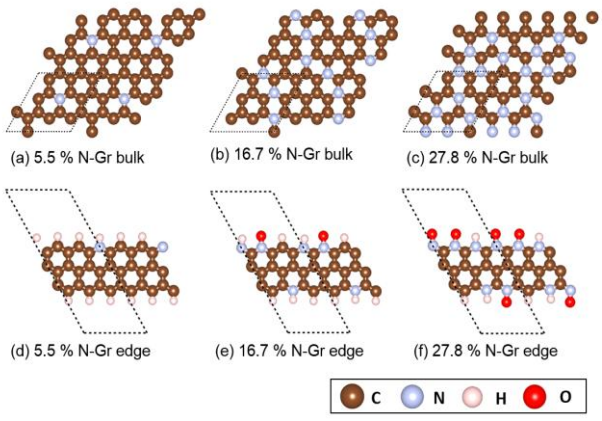

Figure 4. Model bulk and edge N-Gr systems are used in this study to investigate fundamental mechanisms of ORR catalysis. The dashed parallelograms denote the unit cells used in DFT calculations.

The final structures formed after the first ORR processes in edge shapes of N-Gr were illustrated by red-coloured squares in Figure 3. It is a sort of structural poisoning, since the original structures before the ORR started are not recovered via strong chemical bonding (high reduction potentials) with H or O. One thing worthy of noting is that our results on identifying the initial N-Gr structures formed by the first ORR in Figure 3 are purely based on the thermodynamic aspects. Kinetic effects, which could require substantial activation energy to accomplish the proposed reaction chain could essentially block a route or may facilitate other mechanistic paths.

Following this detailed analysis, in Figure 4 we show the bulk (a ~ c) and edge (d ~ f) N-Gr forms with different at.% N that were used to study ORR mechanisms. For the bulk models we adopted the ground state structures as predicted from the energy convex hull shown in Figure 1, while for edge models the configurations marked in the red boxes in Figure 3 were adopted.

Electronic structures of N-Gr model systems

It has been speculated before that N-Gr reduces O_2 from the gas phase to H_2O via a four-electron pathway, while pristine graphene takes part only in a two-electron process which ends up in peroxide generation.[16, 34] These distinct mechanisms have been attributed to the perturbations in the charge distribution caused by the dopant N atoms.[25] We calculated the spatial variation in the distribution of electronic charges in bulk and edge N-Gr using the Bader Charge analysis[35] as shown in Figure 5. It can be clearly seen that there is indeed a substantial amount of charge relocation to N from the first nearest neighbour C atoms, leaving the C atoms partially positive, while N is partially negative. This charge distribution is much more favourable for adsorption of any oxygenated species, because the charge distribution leads to a marked decrease in the repulsive electronic force between the lone pair of the oxygen and the 2 π electrons the carbon atom.

The amount of charge relocation in the edge form is similar to that in the bulk, but the degree of polarization of nearby C atoms is much stronger in the edge form. The same has been confirmed earlier by Luo et al.,[20] who proposed that the strongly polarized C atom at the first nearest neighbour position to N can mitigate the repulsive interaction between N and O_2. We stipulate that such an effect results from two factors. First, there are only two C atoms instead of three as found in the bulk model. Second, due to the poisoning of edge N-Gr forms by oxygen and hydrogen as discussed earlier, the electronic charge is redistributed more towards the nitrogen and oxygen atoms because of their higher electronegativity. This polarization of the nearest neighbour C due to the presence of electronegative groups in the nearest and next nearest neighbour positions possibly also helps in inducing the adsorption of O_2 at the C site.

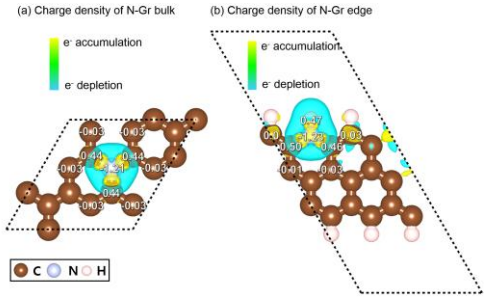

Figure 5. Charge density distribution calculated by Bader's analysis for (a) 5.5 at.% N bulk and in (b) 5.5 at.% N edge N-Gr models.

Thermodynamic free energy diagram of ORR: Formalism

To understand the fundamental mechanisms of ORR in N-Gr, we calculated thermodynamic free energy diagrams for ORR in each of the model systems, as depicted at Figure 4, following the procedure as reported in earlier studies.[30, 36] Factors such as electrode potential, pH, and two thermodynamic variables - the dopant concentration and the morphology (either bulk or edge) directly affect the ORR and were considered in this study. In addition to these factors, we also considered the effect of water solvation by H_2O molecules in the model systems until the density reached 1 gcm^{-3}. Structures of water were optimized using ab-initio molecular dynamics at T = 300 K over a time span of 2 picoseconds.

The Gibb's free energy of each intermediate can be decomposed into several subcomponents as shown in Eq. (3),

$$\Delta G = \Delta E + \Delta ZPE - T\Delta S + \Delta G_U \qquad (3).$$

ΔE is the DFT-calculated total energy of an intermediate, ΔZPE means zero-point energy correction, T is thermodynamic temperature, and ΔS is entropy change, the values of which were borrowed from other sources.[37] We considered the effect of electrode potential (U) as ΔG_U by linearly shifting electronic chemical potential as much as –nFU, as stated by Nernst's law (n is the number of electrons involved at each reaction step). We used ΔZPE and entropy corrections as used in earlier studies at T = 300 K, P = 1 atm and pH =0.[30]

Gibbs free energy diagrams for ORR: The effect of dopant concentration

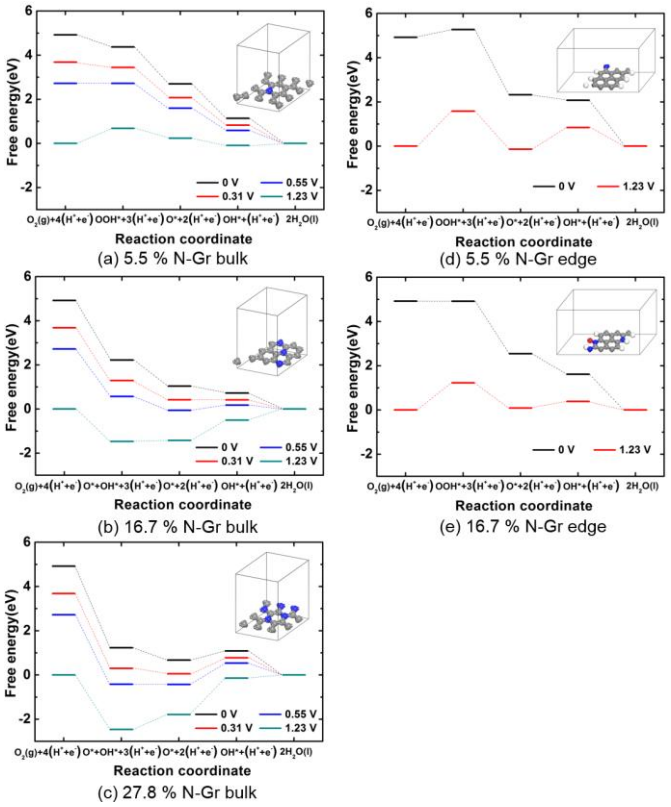

Figure 6. These figures show free energy diagrams of ORR in bulk and edge models with varying at.% N. Here, the effect of water solvation was not considered.

In Figure 6, we show the thermodynamic Gibbs free energy diagrams for ORR for bulk and edged N-Gr as a function of at.% N, but without water solvation. Such an analysis helps in understanding the dependence of ORR on exclusively the binding energy with the catalyst surface. Regardless of composition, our results indicate that the oxygen gas adsorbs associatively on both bulk and edged N-Gr. This is an important distinction to be considered, noting that there is a substantial activation barrier for a pure Gr to adsorb oxygen gas, which is eventually reduced into peroxide at PEM fuel cell operational conditions. We propose that this change in activity can be explained as the result of the partial electronic polarization at C atoms neighbouring the dopant N atoms as described in the section of *Poisoning of dangling bonds in edge N-Gr,* which enables N-Gr to attractively interact with oxygen by lowering the activation barrier for chemical adsorption.

The free energy diagrams in Figure 6 show that the ORR mechanisms in bulk and edged N-Gr are sensitive to dopant concentration and morphology of N-Gr. At 5.5 at.% N, the ORR mechanisms are associative in the N-Gr, but dissociative in all other bulk N-Gr models. This is because the charge deficiency at the C atom also increases as at.% of doped N increases, thus making its bond with the OOH* intermediate much stronger, eventually resulting in the dissociation of OOH* into O* and OH*. We find that onset potential for the electrochemical reduction of O_2 to OOH* at 5.5 at.% N is 0.55 V, at which the free energies of both O_2 and OOH* are equal (i.e. in equilibrium). Over all, the reduction step of O_2 into OOH* in 5.5 at.% N doped bulk N-Gr is likely to have thermodynamically the lowest driving force. While the effect of the doping level on the free energy of OH* is marginal, its impact is crucial on O*. This can be clearly observed in the last two reduction steps in Figures 6(a), (b) and (c). As the at.% N increases, the binding energy of O* increases and that of OH* remains largely unaffected. It shifts thermodynamic tailback to the electrochemical reduction of O* to OH* as at.% N increases. In fact, O* is found to be so strongly stabilized in the 27.8 at.% N model, that there is no ORR activity. Remarkably, it is these different dependencies of O* and OH* on dopant concentration that eventually lead to substantial amounts of overpotential for ORR. The effect of N doping on the onset potentials of ORR in bulk N-Gr is negative: 0.55 V at 5.5 at.% N to 0 V at 27.8 at.% N doped bulk Gr.

ORR mechanisms without solvation in all edged N-Gr are found to be associative, and the free energy for the electrochemical reduction of O_2 to OOH* is uphill in the entire potential range of 0 and 1.23 V. Unfortunately, this result bears similarity with ORR in a pristine graphene, which gives rise to peroxide via the two-electron process. Unlike in bulk N-Gr, the effect of at.% N on ORR efficiency in edged N-Gr is small. Although the Gibbs free energies of intermediates are stabilized as at.% N increases (as shown Figures 6(d, e)), the large overpotential of the first ORR step still remains.

Interestingly, the N-Gr edged form with 27.8 at.% N shows a completely different ORR mechanism than the other models. The ORR pathway for 27.8 at.% N edged N-Gr, as illustrated in Figure 7, shows that even though the edge N atoms are active toward reducing O_2 into OOH*, the chemically poisoned structure energetically forces oxygen gas to adsorb on the C connecting the N atoms, at which it is reduced to OOH* at relatively low potentials below 0.24 V. Further, it was found that the N-Gr framework could be broken during a simultaneous detachment of the chemical bond between C and N and the protonation of OOH* at C resulting into formation of a H_2O molecule. The calculated reversible potential (3.10 V) indicates a high thermodynamic driving force for the reaction at PEM fuel cell operational condition. Kim et al.[23] found the same behaviour. The thermodynamic calculations presented here for further reactions suggest that the broken framework can be eventually restored through a series of chain reactions. The potential window of the reversible reactions is so wide (0.24 ~ 3.10 V) that the breaking and restoring mechanism of the N-Gr framework is of importance as the operational potential of PEM fuel cell is repetitively cycled within this potential range. Our results imply that the structural integrity of a 27.8 at.% doped N-Gr, however, should be very vulnerable to serious degradation, once thermodynamic conditions vary or any kinetic factor becomes important in the ORR process.

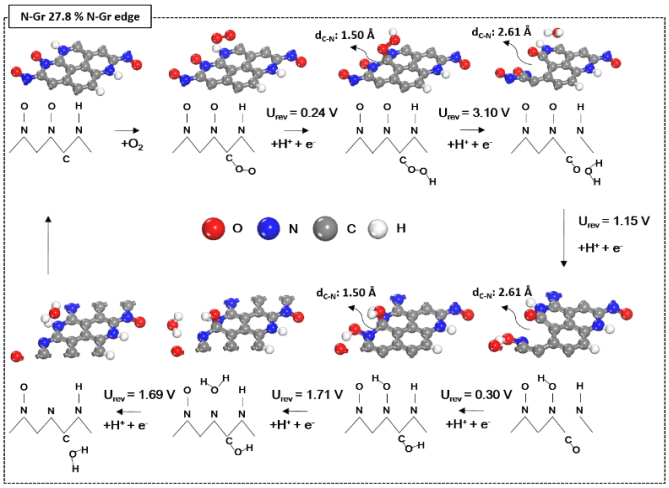

Figure 7. A proposed ORR pathway for the bulk (a) and in (b) the edged form of N-Gr with 27.8 at.% N-doping level. Detailed catalysis cycle for ORR of the edged form of N-Gr was illustrated via a series of electrochemical reaction steps.

To summarize the results for the bulk N-Gr without water solvation, the catalytic efficiency towards ORR decreases as the at.% N increases. The mechanism is dictated mostly by the stabilization of adsorbed O* by the doped N, thus making the reduction of O* into OH* the thermodynamically most difficult step. In other words, the potential energy surface of bulk N-Gr manifests itself in a shape considerably biased towards O* but not OH* or OOH*. In the edged form of N-Gr, thermodynamic efficiency of ORR is found to be worse than in the bulk form, even though the doped N almost stabilizes all of the oxygen containing chemical species. The higher the N doping level is, the worse the ORR activity. This analysis of ORR mechanisms without the solvation effect of water sheds light on the ways the mechanisms could be influenced by the binding energy of the intermediates.

Thermodynamic free energy diagram of ORR: Effect of water solvation

We calculated the thermodynamic Gibbs free energy diagrams of bulk and edged N-Gr models exposed to a water environment. We placed 16 and 39 H_2O molecules in bulk and edged form of N-Gr model systems, respectively, to make the water density 1 gcm^{-3} in each. The water structure was then optimized using ab-initio molecular dynamics for 2 picoseconds at T = 300 K.

Figure 8 illustrates the calculated thermodynamic free energy diagrams of ORR in the bulk and edged N-Gr models under water solvation. In case of bulk N-Gr, although the Gibbs free energies of ORR intermediates shift to more negative values (implying higher stabilization), the overall trends largely remain the same as those without water solvation. The onset potential for ORR at 5.5 at.% N in the bulk form increases from 0.55 V to 0.79 V after inclusion of a water environment (as shown in Figures. 6 (a) and 8 (a)). We propose that such an effect arises as a result of the thermodynamic stabilization of adsorbed OOH* by the surrounding H_2O molecules, which lowers the onset potential for reduction of O_2. This result is in good agreement with experiments.[17-19, 21] In total, the effect of dopant N atoms stabilizing adsorbed oxygen atoms is dominant over the impact of water solvation, because the effect of solvation due to water molecules in bulk N-Gr model is similar across all intermediates.
In the edge N-Gr model, although the adsorbed OOH* species becomes slightly stable at 5.5 and 16.7 at.% N doping levels (as shown in Figures. 6(d, e) and 8(d, e)), the first reduction step of O_2 to OOH* with water molecules is still found to face a large overpotential for the first reaction step. Unfortunately, the onset potentials for ORR at the edged form of N-Gr are almost zero with water. Although the presence of dopant and water solvation lead to possible stabilization of the intermediates, the weak adsorption of OOH species at edged N-Gr leads to a very large overpotential. This seems to suggest that ORR will not be feasible on the edge forms of doped N-Gr. These findings agree well with recent experiments.[20, 21, 38, 39]

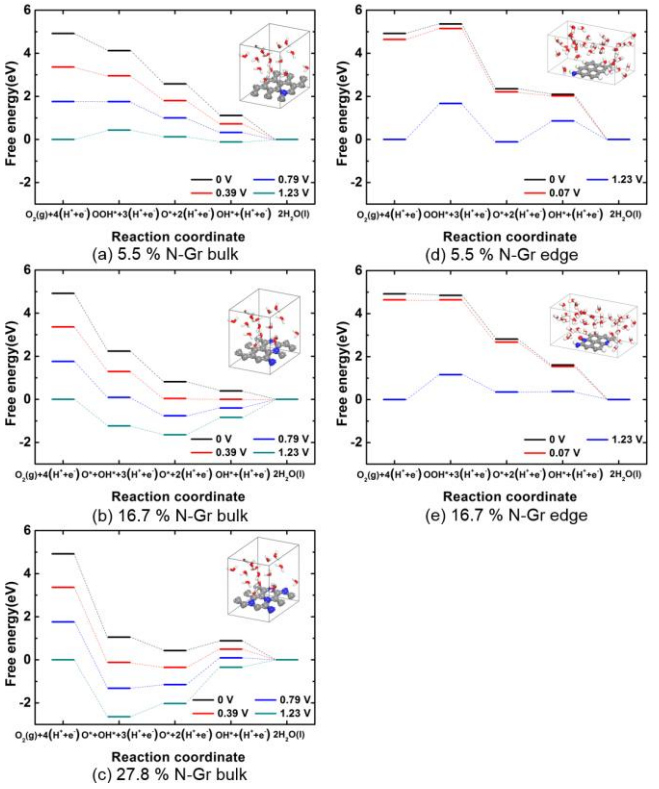

Figure 8. Free energy diagrams of ORR in bulk and edge N-Gr models with varying number of doped N atom taking into account the effect of solvation due to water.

Conclusion

Using first principles DFT calculations, we analysed catalytic activity of N-Gr toward ORR, which is found to be significantly influenced by atomistic morphology and concentration of dopant N atoms. A rigorous process to identify the thermodynamically most stable structures was employed for bulk and edge shapes of N-Gr, after which poisoning of the edged form N-Gr under a reducing environment was also considered in detail. Without the effect of aqueous solvation, the catalytic efficiency towards ORR is found to be mostly controlled by the strong chemical stabilization of adsorbed O* in bulk N-Gr due to the dopant N, thus making the reduction of O* into OH* thermodynamically the most difficult step. The phenomenon is more conspicuous in edged forms of N-Gr leading to even lower ORR onset potentials than in bulk N-Gr. The effect of water solvation on ORR activity is stronger at dilute N doping levels and diminishes as the N concentration increases. Thus, the solvation by water molecules contributes only marginally to controlling ORR activity of N-Gr compared with the effect of N-doping. Based on these findings, we propose that bulk form N-Gr catalysts with dilute N concentration are more optimized towards ORR catalysis. The extensive analysis of finding stable structure and determining ORR mechanism present in this study is useful for rational design of promising non-precious catalysts, and can also be applied to other areas where one hopes to upgrade the parent material properties by a heteroatom doping.

Model Systems and Computational Details

The model system for pure graphene was set up with a single layer of (3×3) hexagonal graphene framework. Then the dopant N atoms were allowed to substitute the C atoms to make N-Gr sheets. All energy calculations in our models were performed using VASP.[40, 41] Projector Augmented Wave (PAW) pseudo-potentials[42] as implemented in VASP were used for describing the interactions between ions and electrons, and the exchange-correlation energy of electrons was described by employing the generalized gradient approximation (GGA) using the Perdew-Burke-Ernzerhof (PBE) functionals.[43] Van der Waals (vdW) corrections were performed using the Grimme scheme.[44] The Kohn-Sham orbitals were expanded on a plane wave basis set with a cutoff energy of 520 eV. All atoms were fully relaxed until the sum of forces was less than 10^{-4} eV/Å. To integrate the Brillouin zone, a gamma point mesh with 5×5×1 k-points was used and periodic boundary conditions were imposed on the N-Gr models with a large vacuum space of 14 Å in the direction perpendicular to graphene surface for the bulk and edge N-Gr forms. An additional 11 Å were added in the direction perpendicular to the edge but in the same plane for the edged sheets to preclude interactions with images.

Acknowledgements

This work was supported by the Global Frontier R&D Program (2013-073298) on Center for Hybrid Interface Materials (HIM), funded by the Ministry of Science, ICT & Future Planning. Authors also thank the Leading Foreign Research Institute Recruitment Program through the National Research Foundation of Korea (NRF), funded by the Ministry of Education, Science and Technology (MEST) (2012K1A4A3053565) and the New and Renewable Energy R&D Program (20113020030020) under the Ministry of Knowledge Economy, Republic of Korea. Abhishek Khetan gratefully acknowledges the funding of his doctoral studies by the Deutsche Forschungsgemeinschaft (DFG).

Keywords: First principles • Renewable energy • Graphene • Catalyst • Oxygen reduction reaction

[1] F. Studt, I. Sharafutdinov, F. Abild-Pedersen, C. F. Elkjær, J. S. Hummelshøj, S. Dahl, I. Chorkendorff, J. K. Nørskov, *Nat. Chem.* **2014**, 10.1038/nchem.1873.
[2] X. Wang, K. Maeda, A. Thomas, K. Takanabe, G. Xin, J. M. Carlsson, K. Domen, M. Antonietti, *Nat. Mater.* **2009**, *8*, 76-80.
[3] L. Yu, X. Pan, X. Cao, P. Hu, X. Bao, *J. Catal.* **2011**, *282*, 183-190.
[4] P. G. Bruce, S. A. Freunberger, L. J. Hardwick, J.-M. Tarascon, *Nat. Mater.* **2012**, *11*, 19-29.
[5] Z. Peng, S. A. Freunberger, Y. Chen, P. G. Bruce, *Science* **2012**, *337*, 563-566.
[6] M. K. Debe, *Nature* **2012**, *486*, 43-51.
[7] B. C. Steele, A. Heinzel, *Nature* **2001**, *414*, 345-352.
[8] S. H. Noh, M. H. Seo, J. K. Seo, P. Fischer, B. Han, *Nanoscale* **2013**, *5*, 8625-8633.
[9] M. Grätzel, *Nature* **2001**, *414*, 338-344.
[10] A. I. Boukai, Y. Bunimovich, J. Tahir-Kheli, J.-K. Yu, W. A. Goddard Iii, J. R. Heath, *Nature* **2008**, *451*, 168-171.
[11] X. Wang, X. Li, L. Zhang, Y. Yoon, P. K. Weber, H. Wang, J. Guo, H. Dai, *Science* **2009**, *324*, 768-771.
[12] D. J. Norris, A. L. Efros, S. C. Erwin, *Science* **2008**, *319*, 1776-1779.
[13] L. Zhao, R. He, K. T. Rim, T. Schiros, K. S. Kim, H. Zhou, C. Gutiérrez, S. Chockalingam, C. J. Arguello, L. Pálová, *Science* **2011**, *333*, 999-1003.
[14] A. Rabis, P. Rodriguez, T. J. Schmidt, *ACS. Catal.* **2012**, *2*, 864-890.
[15] H. Wang, T. Maiyalagan, X. Wang, *ACS. Catal.* **2012**, *2*, 781-794.
[16] L. Qu, Y. Liu, J.-B. Baek, L. Dai, *ACS nano* **2010**, *4*, 1321-1326.
[17] D. Geng, Y. Chen, Y. Chen, Y. Li, R. Li, X. Sun, S. Ye, S. Knights, *Energy Environ. Sci.* **2011**, *4*, 760-764.
[18] C. H. Choi, M. W. Chung, H. C. Kwon, S. H. Park, S. I. Woo, *J. Mater. Chem. A* **2013**, *1*, 3694-3699.
[19] C. H. Choi, S. H. Park, S. I. Woo, *ACS nano* **2012**, *6*, 7084-7091.
[20] Z. Luo, S. Lim, Z. Tian, J. Shang, L. Lai, B. MacDonald, C. Fu, Z. Shen, T. Yu, J. Lin, *J. Mater. Chem.* **2011**, *21*, 8038-8044.
[21] Y. Zhang, J. Ge, L. Wang, D. Wang, F. Ding, X. Tao, W. Chen, *Sci. Rep.* **2013**, *3*.
[22] K. Parvez, S. Yang, Y. Hernandez, A. Winter, A. Turchanin, X. Feng, K. Mu□llen, *ACS nano* **2012**, *6*, 9541-9550.
[23] H. Kim, K. Lee, S. I. Woo, Y. Jung, *Phys. Chem. Chem. Phys.* **2011**, *13*, 17505-17510.
[24] Y. Okamoto, *Appl. Surf. Sci.* **2009**, *256*, 335-341.
[25] L. Zhang, Z. Xia, *J. Phy. Chem. C* **2011**, *115*, 11170-11176.
[26] X. Fan, W. Zheng, J.-L. Kuo, *RSC. Adv.* **2013**, *3*, 5498-5505.
[27] A. A. F. Van der Ven, PhD thesis, Massachusetts Institute of Technology **2000**.
[28] A. Y. Liu, R. M. Wentzcovitch, *Phy. Rev. B* **1994**, *50*, 10362.
[29] S. Souto, M. Pickholz, M. Dos Santos, F. Alvarez, *Phy. Rev. B* **1998**, *57*, 2536.
[30] J. K. Nørskov, J. Rossmeisl, A. Logadottir, L. Lindqvist, J. R. Kitchin, T. Bligaard, H. Jonsson, *J. Phy. Chem. B* **2004**, *108*, 17886-17892.
[31] K. A. Kurak, A. B. Anderson, *J. Phy. Chem. C* **2009**, *113*, 6730-6734.
[32] D. Geng, S. Yang, Y. Zhang, J. Yang, J. Liu, R. Li, T.-K. Sham, X. Sun, S. Ye, S. Knights, *Appl. Surf. Sci.* **2011**, *257*, 9193-9198.
[33] Y. Wang, Y. Shao, D. W. Matson, J. Li, Y. Lin, *Acs Nano* **2010**, *4*, 1790-1798.
[34] Y. Jiao, Y. Zheng, M. Jaroniec, S. Z. Qiao, *JACS.* **2014**, *136*, 4394-4403.
[35] W. Tang, E. Sanville, G. Henkelman, *J. Phys.: Condens. Matter* **2009**, *21*, 084204.
[36] B. Han, V. Viswanathan, H. Pitsch, *J. Phy. Chem. C* **2012**, *116*, 6174-6183.
[37] P. Atkins, *Physical Chemistry, 6th Edition, Oxford, U.K.*, **1998**, pp. 485, 925-927, 942.
[38] R. A. Sidik, A. B. Anderson, N. P. Subramanian, S. P. Kumaraguru, B. N. Popov, *J. Phy. Chem. B* **2006**, *110*, 1787-1793.
[39] Y. Shao, J. Sui, G. Yin, Y. Gao, *Appl. Catal. B* **2008**, *79*, 89-99.
[40] G. Kresse, J. Furthmüller, *Comput. Mater. Sci.* **1996**, *6*, 15-50.
[41] G. Kresse, J. Hafner, *Phy. Rev. B* **1993**, *47*, 558.
[42] P. E. Blöchl, *Phy. Rev. B* **1994**, *50*, 17953.
[43] J. P. Perdew, K. Burke, M. Ernzerhof, *Phy. Rev. Lett.* **1996**, *77*, 3865.
[44] S. Grimme, *J. Comput. Chem.* **2006**, *27*, 1787-1799.

Received: ((will be filled in by the editorial staff))
Published online: ((will be filled in by the editorial staff))

Entry for the Table of Contents (Please choose one layout only)

Layout 1:

FULL PAPER

Text for Table of Contents.

N-Gr for ORR: Oxygen reduction reaction (ORR) is examined on 5.5, 16.7 and 27.8 at.% N doped graphene bulk and edge. Dilutely (5.5 at.% N) doped bulk N-Gr exhibits the best ORR activity in our DFT calculations, and high N concentration (27.8 at % N) leads to the break of graphene frame as shown in graphical abstract

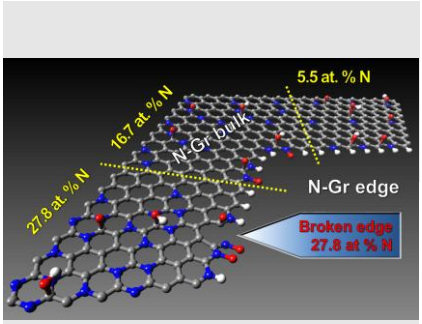

DoHyun Kwak[a], Abhishek Khetan[b], SeungHyo Noh[c], Heinz Pitsch[b], Byungchan Han[a]*

Page No. – Page No.

Title

First principles study of morphology, doping level and water solvation effects on catalytic mechanisms of graphenes towards oxygen reduction reaction

Layout 2:

FULL PAPER

((The TOC Graphic should not exceed the size of this area))

*Author(s), Corresponding Author(s)**

Page No. – Page No.

Title

Text for Table of Contents.

Text for Table of Contents----continued.